

Intra-seasonal variability of Pacific-origin sea level anomalies around the Philippine Archipelago

Xiao Chen^{1,2,3} · Bo Qiu³ · Xuhua Cheng¹ · Yiquan Qi¹ · Yan Du¹

Received: 1 October 2014 / Revised: 23 February 2015 / Accepted: 2 March 2015 / Published online: 20 March 2015
© The Oceanographic Society of Japan and Springer Japan 2015

Abstract Intra-seasonal variability of sea level anomalies (SLAs) originated in the Pacific Ocean around the Philippine Archipelago was investigated using merged altimetry SLA measurements and eddy-resolving ocean model outputs. The results suggest the SLA signals from the tropical North Pacific propagate westward as baroclinic Rossby waves on an intra-seasonal time scale. Upon impinging the east coast of the Philippines, these Rossby wave signals transform into coastal trapped waves (CTWs), propagate clockwise along the coast of the Philippine Archipelago and enter into the eastern South China Sea (SCS) through the Sibutu Passage and Mindoro Strait. The SLA signals, however, cannot propagate anticlockwise and enter into the eastern SCS through the Luzon Strait. The intra-seasonal oceanic wave processes are clearly identified by the eddy-resolving model. The effect of along-shore wind forcing on the SLA signals appears insignificant when compared with the remote signals coming from the interior Pacific. While identified in the model simulation, future observations are needed to verify the intra-seasonal CTWs encircling the Philippine Archipelago.

Keywords Intra-seasonal variability · Sea level anomaly · Philippines · South China Sea · Rossby wave · Coastal trapped wave

✉ Yan Du
duyan@scsio.ac.cn

¹ State Key Laboratory of Tropical Oceanography (LTO), South China Sea Institute of Oceanology, Chinese Academic of Science, 164 West Xingang Road, Guangzhou 510301, China

² Graduate University of Chinese Academy of Sciences, Beijing, China

³ Department of Oceanography, University of Hawaii at Manoa, Honolulu, HI, USA

1 Introduction

The Philippine Archipelago is a critical region that plays an important role in the oceanic exchanges between the South China Sea (SCS) and the western Pacific. This region is characterized by multi-connected ocean passages and channels (Fig. 1). To the north, the Luzon Strait (sill depth ~2,200 m) is the main oceanic linkage of the SCS and the western Pacific. To the south, the Mindoro (sill depth of ~500 m) and the shallow Balabac Straits connect the Sulu Sea and the SCS. The Sibutu Passage (deeper than 200 m) connects the Sulu and Sulawesi Seas. The monsoonal winds dominate the region, with southwesterly winds prevailing during the boreal summer and northeasterly winds during the boreal winter (Wyrtki 1961). With a complex ocean bathymetry, the dynamical processes around the region are equally complex.

Previous studies reveal that the water mass and energy exchanges between the SCS and the western Pacific in the vicinity of the Philippine Archipelago vary on a wide range of spatio-temporal scales (e.g., Wyrtki 1961; Nitani 1972; Metzger and Hurlburt 1996; Qiu and Lukas 1996; Qiu and Chen 2010, 2012; Hsin et al. 2012). Along the east coast of the Philippines, the North Equatorial Current (NEC) bifurcates into the northward Kuroshio and the southward Mindanao currents (the NMK system). Variations of the NMK system on the seasonal to multi-decadal time scales exert a large impact on the circulations around the archipelago (e.g., Nitani 1972; Toole et al. 1990; Qiu and Lukas 1996; Kim et al. 2004; Liang et al. 2008; Qiu and Chen 2010, 2012). Dynamically, a northward shift of the bifurcation latitude in the NEC favors the intrusion of the Kuroshio into the SCS, corresponding to a larger Luzon Strait transport (LST) (Sheremet 2001). Observations and model results suggest that the LST is westward

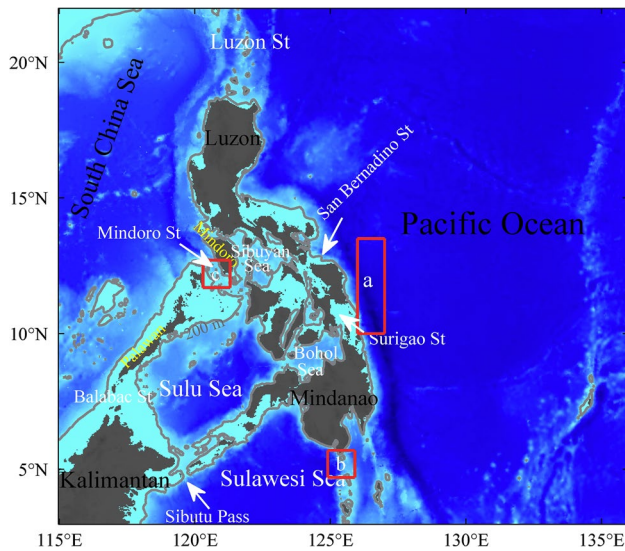


Fig. 1 Bathymetry around the Philippine Archipelago, with 200-m contours plotted as white lines. Sea level anomalies (SLAs) in box a, b and c are used for spectral analysis

in the climatological mean state and reaches a maximum in the winter (westward) and a minimum in the summer (eastward) (e.g., Wyrski 1961; Shaw 1991; Metzger and Hurlburt 1996; Qu et al. 2004; Liang et al. 2008; Hsin et al. 2012). On interannual time scales, the LST is closely related to the El Niño-Southern Oscillation (ENSO) in the tropical Pacific, being higher (lower) during the El Niño (La Niña) events (e.g., Qu et al. 2004; Wang et al. 2006; Cheng and Qi 2007; Liang et al. 2008; Du and Qu 2010). To the south, the annual mean surface currents enter from the SCS to the Sulu Sea at the Mindoro and Balabac Straits and exit from the Sulu Sea to the Suluwesi Sea at the Sibutu Passage (e.g., Metzger and Hurlburt 1996; Sprintall et al. 2012). Surface water near the San Bernardino and Surigao Straits flows westward and constitutes a direct pathway that conveys the surface water from the western Pacific to the Sulu Sea (e.g., Wyrski 1961; Metzger and Hurlburt 1996; Han et al. 2008; Sprintall et al. 2012).

Figure 2a and b compare the observed monthly sea level variations in the eastern SCS vs. those in the western Pacific near the NEC bifurcation (see white boxes for their locations). It is easy to discern the temporal similarities between the two time series. Figure 2c shows the difference map between the positive-minus-negative sea level composites that exceed one standard deviation (dotted lines in Fig. 2a and b). There exists a clear synchronous sea level variation along the eastern and western coasts of the Philippine archipelagos. Dynamically, this synchronous sea level variation is the result of various time-scale processes from days to years. On the interannual-to-decadal time scales, it can be partly explained by the close relationship of the SCS

monsoon with the ENSO through atmospheric teleconnection, in the form of an anomalous anticyclonic circulation in the lower-troposphere over the western North Pacific (Wang et al. 2000; Fang et al. 2006; Xie et al. 2009). In fact, the low-frequency varying winds over the North Pacific tropical gyre dominate the interannual-to-decadal variations of the sea level and circulation around the Philippines Islands (e.g., Qiu and Chen 2010; Zhuang et al. 2013). In addition, oceanic passages contribute to the synchronous variations of the eastern SCS and the western Pacific through wave motions (Liu et al. 2011; Zhuang et al. 2013). On the interannual time scales, for example, the ENSO signals can propagate into the eastern SCS via the low-latitude channels in the form of CTWs (Liu et al. 2011).

So far, rapid processes of sea level signals propagating from the western Pacific into the eastern SCS have not been fully explored. High-frequency oceanic processes, however, can impact the regional ecological and biogeochemical conditions (e.g., Amedo et al. 2002). High-frequency sea level oscillations in the eastern SCS can also influence the meridional pressure gradient across the Luzon Strait, hence the LST. Our study is focused on the intra-seasonal variations of sea level anomalies (SLAs) around the Philippine Archipelago. The possible influence of local winds around the Philippine coast is also evaluated.

It is still controversial as to whether sea level signals originated in the interior Pacific can penetrate the Kuroshio and propagate into the northern SCS through the Luzon Strait (Hu et al. 2001, 2012; Li et al. 2007; Zhang et al. 2010; Lu and Liu 2013). As will be discussed in this study, the Pacific-origin, intra-seasonal sea level signals cannot enter the eastern SCS directly through the Luzon Strait in the form of oceanic waves.

The rest of the paper is organized as follows. Section 2 describes the datasets and methods. Section 3 investigates the processes of the Pacific-origin sea level signals entering the eastern SCS. Section 4 provides discussion and a summary.

2 Data

2.1 Observational data

Merged SLA data derived from simultaneous measurements of two satellites (TOPEX/Poseidon or Jason-1 and ERS or Envisat) is used in this study. The data is distributed by Archiving, Validation, and Interpretation of Satellite Oceanographic data (AVISO <http://www.aviso.oceanobs.com/>). Using two satellites instead of one greatly improved the data quality of the mesoscale signals (Le Traon and Dibarboure 1999). In order to correct the aliasing of tides and barotropic variability, the altimeter dataset was updated

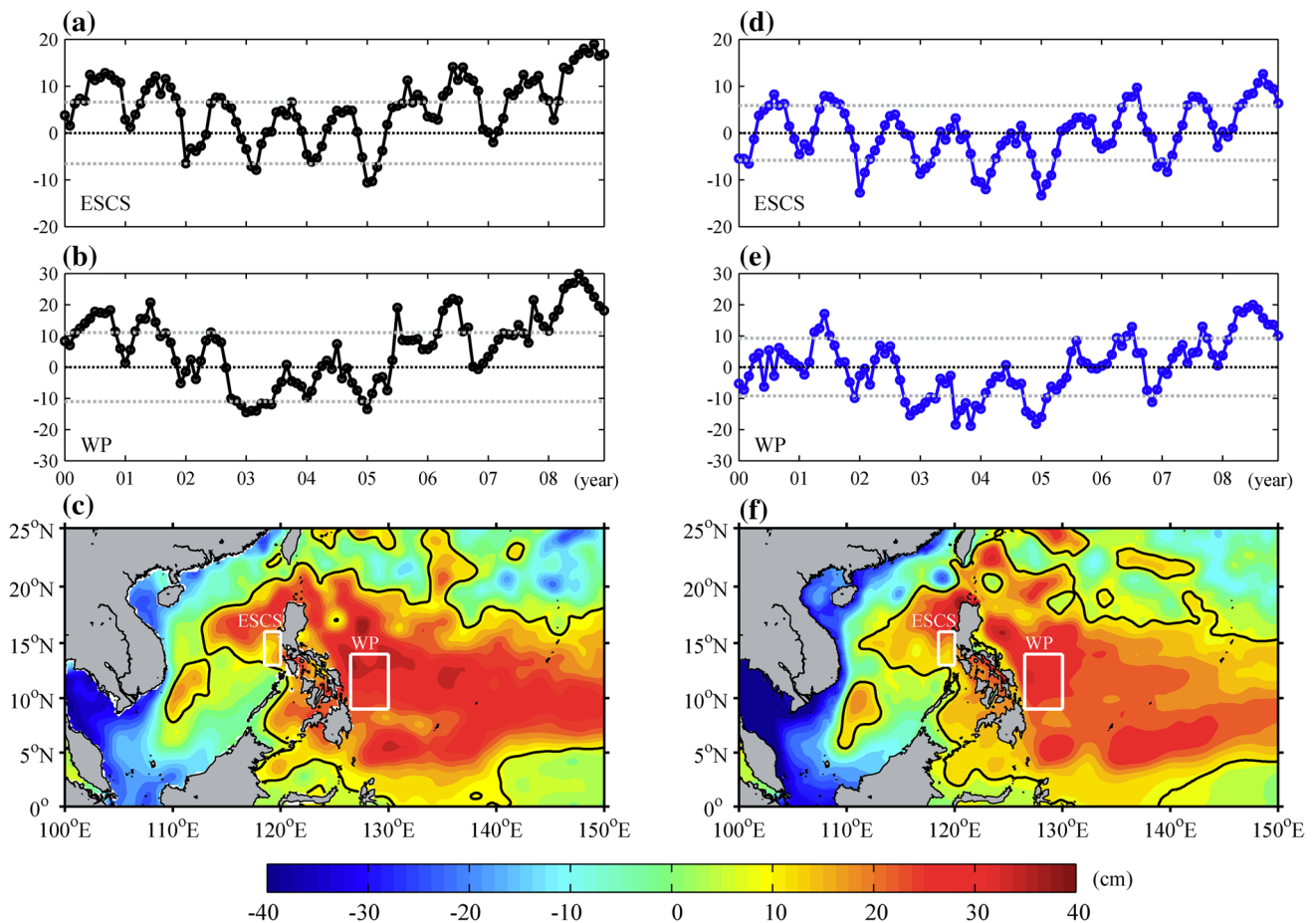


Fig. 2 Monthly sea level time series boxes in **a** the eastern ECS and **b** the western Pacific, from the AVISO data product. **c** Difference between positive-minus-negative composites that exceed one standard deviation. **d–f** Same as (a–c) except for from the QSCAT run of 2000–2008

with new corrections from 2005 using a new tidal model (GOT2000, Goddard/Grenoble Ocean Tide) and a barotropic model (MOG2D-G, Modèle aux Ondes de Gravité 2-Dimensions Global) (Volkov et al. 2007; Dibarbouré et al. 2008). The product is available on the 1/3° mercator grid at a weekly interval and then interpolated to daily values using cubic splines. Sea surface wind data used in this study is from the QuikSCAT microwave scatterometer (Wentz et al. 2001), available from the Asia-Pacific Data-Research Center (APDRC) with a daily interval (three-day running mean) and on a 1/4° grid.

2.2 Eddy-resolving model

Results from the eddy-resolving Oceanic General Circulation Model (OGCM) for the Earth Simulator (OFES) (Masumoto et al. 2004; Sasaki et al. 2004) are used. The model is based on the Modular Ocean Model (MOM3) (Pacanowski and Griffies 2000), with a near-global domain extending from 75°S to 75°N. Its horizontal resolution is 0.1° with 54 vertical levels.

The model is initialized from a state of rest with annual mean temperature and salinity fields of the World Ocean Atlas 1998 (WOA98) (Boyer and Levitus 1997). It is spun up for 50 years with monthly climatological forcing. Wind stress, heat and fresh water fluxes utilized in the model are derived from the National Centers for Environmental Prediction/National Center for Atmospheric Research (NCEP/NCAR) reanalysis for 1950–1999 (Kalnay et al. 1996). At the surface, additional restoring to the monthly mean sea surface salinity (SSS) of WOA98 is imposed.

Following the spin-up integration, a hindcast simulation from 1950 to 2005 is conducted with daily atmospheric forcing from the NCEP/NCAR reanalysis (NCEP run). Evaporation and precipitation are from the daily NCEP/NCAR reanalysis. Another hindcast starts from the NCEP run on July 1999 but is forced by daily mean surface wind stress from QuikSCAT measurements (QSCAT run; Sasaki and Nonaka 2006). This study uses the QSCAT run, the performance of which is better than the NCEP run because of the high resolution and a more accurate wind product (Zhuang et al. 2010; Cheng et al. 2013). The QSCAT run outputs from 22

July 1999 to 30 October 2009 are saved every three days and the sea surface height fields from 2000 to 2008 are used in this study. The OFES SLA fields are obtained by subtracting the modeled mean sea surface height field of 2000–2008.

In order to extract the high frequency SLA variations, we removed signals from the semiannual and annual cycles, and the interannual-to-decadal signals. Variations with periods shorter than two weeks are highly correlated to weather processes that are also removed before further analyses. After pre-processing, power spectral analysis is carried out for the SLA values averaged in the three representative boxes around the archipelago (see their locations in Fig. 1). There exist statistically significant signals in the 30–120 day band (Fig. 3) and these intra-seasonal (30–120 day) signals are the focus of the following analyses.

3 Origin of intra-seasonal SLAs in the eastern SCS

3.1 Intra-seasonal SLAs around the Philippine Archipelago

In this section, the evolution of intra-seasonal SLAs is investigated using a regression analysis, with the SLAs referenced to a site off the west coast of Luzon Island (119°E–120°E, 15°N–16°N), as shown in Fig. 4a. At day -21 (Fig. 4a), a positive (A1) and a negative (C1) SLA signals appear at about 127°E, 11°N, and 130°E, 12°N, respectively, and propagates westward. When the positive SLA signal A1 encounters the east coast of the Philippines, part of the energy propagates clockwise along the coast and the SLA phase there rapidly turns positive (Fig. 4c). A1 finally enters the eastern SCS through the Sibutu Passage and Mindoro Strait (Fig. 4d). With A1 continually propagating into the eastern SCS, positive SLA signals along the west coast of the Philippines becomes stronger (Fig. 4d, e). At day $+9$, negative SLA signal C1 encounters the coast and goes through the same pathway as A1 (Fig. 4e–h). Regression analysis of the wind stress, with the same reference location as the SLA, is also superimposed. Off the west coast of the Luzon Island, it is interesting to see the SLAs change from negative to positive from day -21 day to day -3 , while the surface wind stresses fluctuate from northeasterly to southwesterly. This suggests that the intra-seasonal SLA signals along the Philippine coast could potentially be affected by the along-shore wind; this effect will be quantitatively examined in Sect. 4.

3.2 Transformation of intra-seasonal SLA signals

In the propagating intra-seasonal SLA signals (Fig. 4), A1, C1 and A2 originate at about 12°N before they reach

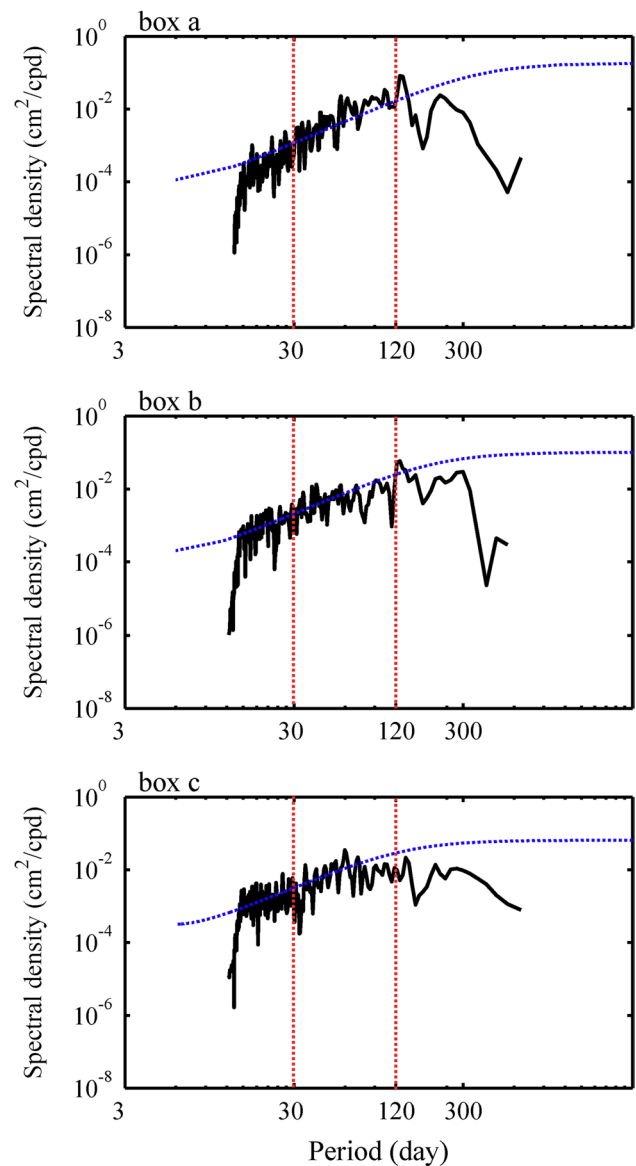


Fig. 3 Power spectra of SLAs from the QSCAT run (with semiannual, annual, and interannual-to-decadal signals removed) in *box a*, *b* and *c*, respectively. Locations of the *boxes* are shown with *red boxes* in Fig. 1. The 95 % confidence levels are shown by *blue dashed lines*, and the *red lines* indicate the cutoff period (30–120 day) for intra-seasonal signals

the Philippine coast. The standard deviation of the intra-seasonal SLA signals (figure not shown) also displays a regionally large value at about 12°N. In this section, we select one typical waveguide to investigate the behavior of propagation in detail (Fig. 5a).

The first half of the selected waveguide (stations 1–14) takes the average between 10°N and 13.5°N at 1° zonal intervals. The rest takes 1° × 1° boxes along the coast of the Philippine Archipelago. Station 7 (Fig. 5a) is chosen as the reference site for the incoming SLA signals. The SLA signals

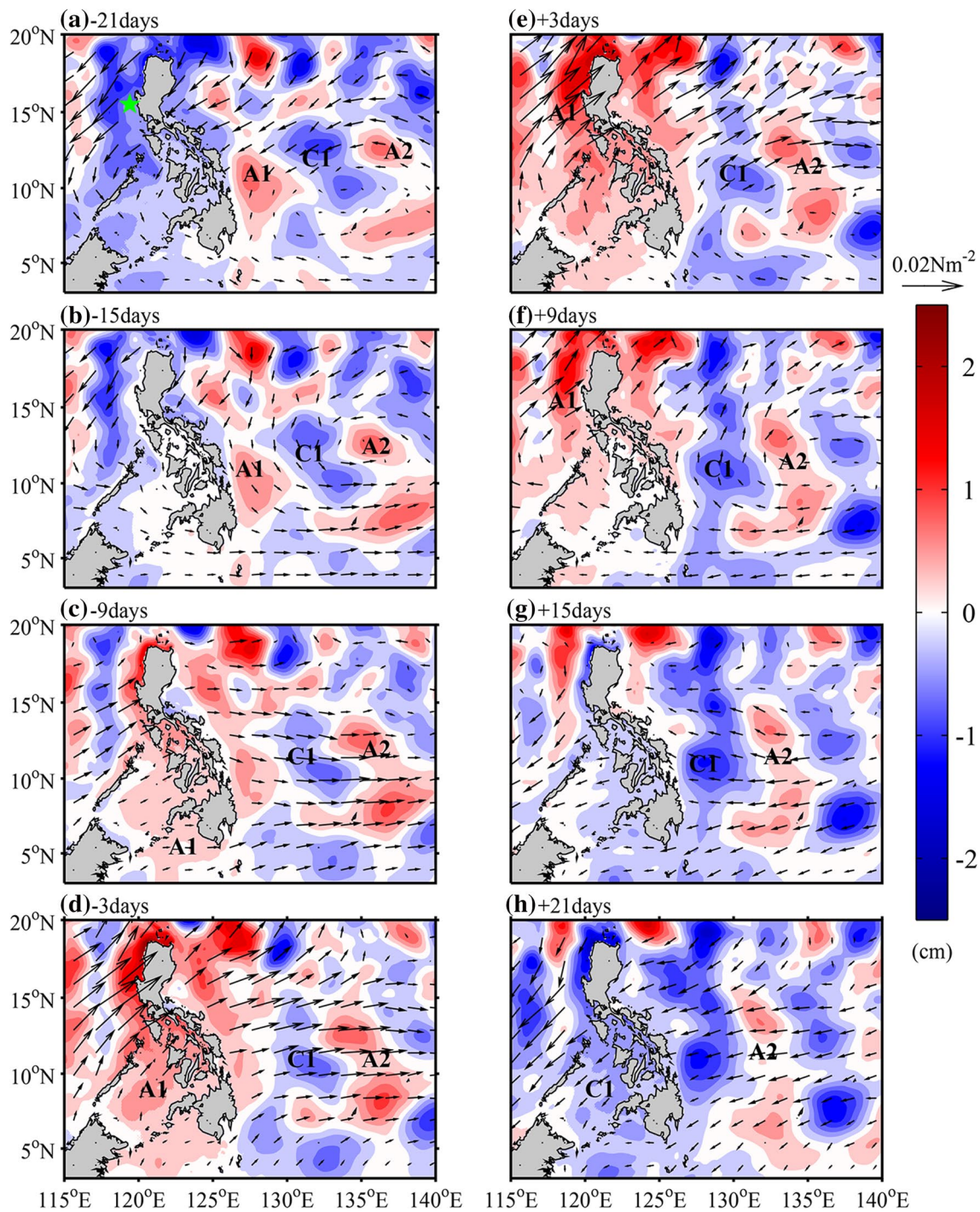


Fig. 4 Lead-lag regression of intra-seasonal SLAs (cm) from the QSCAT run and QuikSCAT wind stress upon on the normalized intra-seasonal SLAs and meridional component of wind stress within the

reference box (119°–120°E, 15°–16°N), noted by green star. Patterns leading by 21, 15, 9 and 3 days, and lagging by 3, 9, 15 and 21 days are shown. The 95 % confidence level has a SLA value of 0.07 cm

propagate westward with a speed of ~ 0.17 m/s from satellite observations (Fig. 5b), and ~ 0.15 m/s from the QSCAT run (Fig. 5c). This speed is close to the theoretical value of the first baroclinic mode Rossby wave at this latitude, ~ 0.11 m/s. Previous studies also indicated that the theoretical phase

speed of the Rossby wave is slower than the observed results outside of 10°S–10°N (e.g., Chelton and Schlax 1996). This confirms that the intra-seasonal SLA signals from the western Pacific propagate westward as baroclinic Rossby waves till they reach the Philippine coast (before station 14).

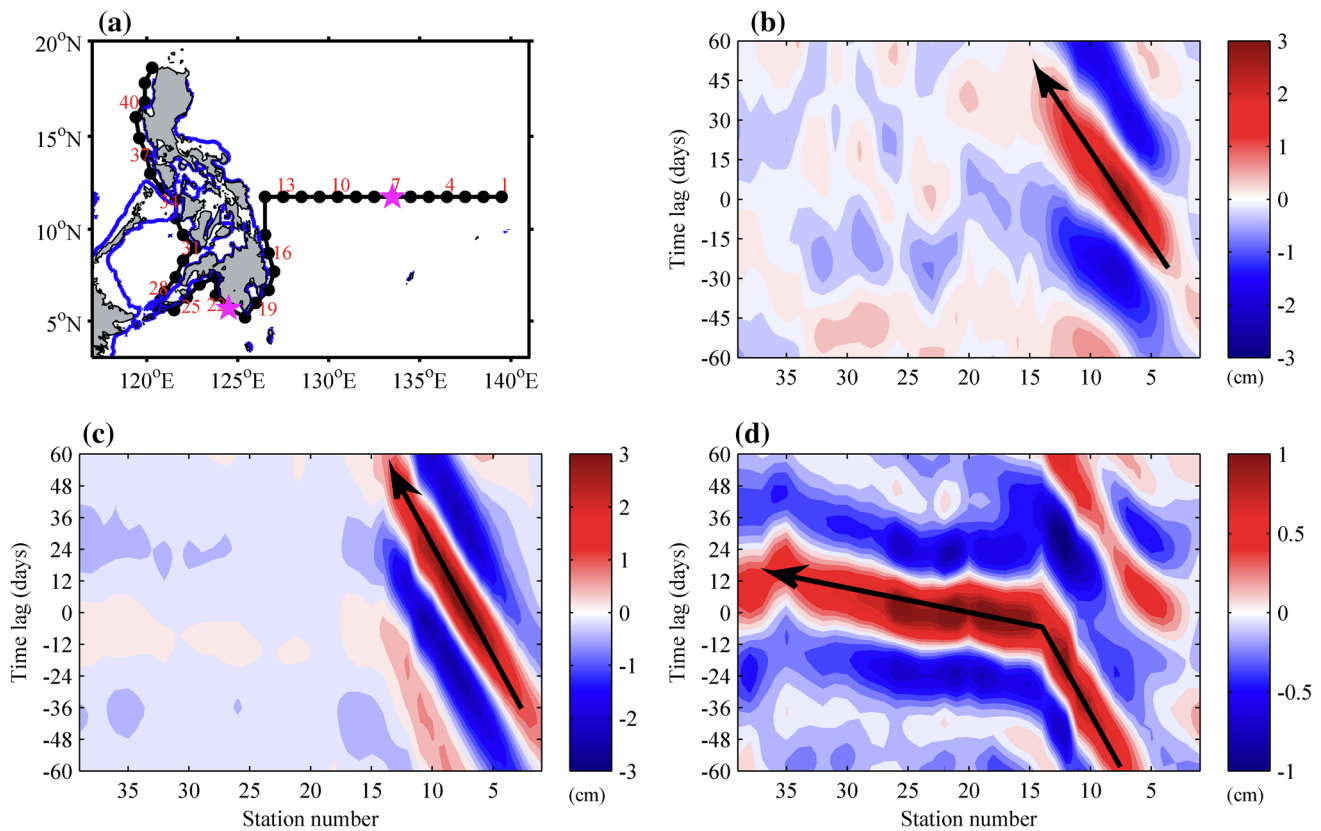


Fig. 5 **a** Distribution of 1° boxes along the waveguide, with the 100-m contours plotted. **b** Corresponding time-station diagram of lead-lag regression of the satellite-observed intra-seasonal SLAs (cm) with respect to the normalized values at station 7. **c** Same as (**b**),

except for the QSCAT run. **d** Same as (**c**), except that the reference site is changed to station 21. For (**b**), (**c**) and (**d**), the 95 % confidence level has a SLA value of 0.07, 0.1 and 0.1 cm, respectively

When station 21 (Fig. 5a) is taken as the reference site along the Philippine coast, an abrupt change from ~ 0.15 m/s to ~ 2.2 m/s occurs in the SLA propagating speed and this change is clearly seen in the high resolution model outputs (Fig. 5d). The increased phase speed agrees with that of the first mode gravity wave in this region, about 2.6–2.8 m/s (Chelton et al. 1998). Given the steep topography along the east coast of the Philippine Archipelago, the oceanic waves should behave more as CTWs than shelf waves. This sudden transformation implies that the SLA signals travel first as baroclinic Rossby waves and then transform into CTWs. When the SLA signals propagate as CTWs, the energy is reduced when moving around the south tip of the Philippine Archipelago (close to station 20); such energy loss is partially related to friction and partially to the gravity wave scattering (Durland and Qiu 2003). Notice that the satellite SSH observation is not suitable for detecting the CTWs for two reasons. First, due to the difficulty in removing near-shore tidal signals, the AVISO altimetric data is less accurate along the Philippine coast. Secondly, the weekly resolution of the satellite data is not high enough to properly capture the fast propagating CTWs.

It is worth noting that the latitude band of the Luzon Strait is another channel with a large amplitude of intra-seasonal SLA variations. This issue will be considered specifically in Sect. 4.

3.3 Interannual variations of SLA propagation

Figure 6 displays the time-dependent variations of the OFES SLA signals along the waveguide indicated in Fig. 5a. It shows clear interannual variations in the propagation of the Pacific-origin SLA signals. In some years (e.g., 2000, 2003, 2004 and 2007), the Pacific-origin SLA signals are stronger. As a result, transformation of the baroclinic Rossby waves to CTWs is clearer. In contrast, the SLA signals are weak in other years (e.g., 2008). These interannual variations are likely linked to the large scale dynamic processes in the Pacific, such as the ENSO (Liu et al. 2011; Zhuang et al. 2013). Although transformations of the SLA signals are clear in many cases (marked with yellow dashed lines in Fig. 6), many others are disrupted, implying possible impacts of nonlinear processes prevalent along the low-latitude western boundary of the Pacific

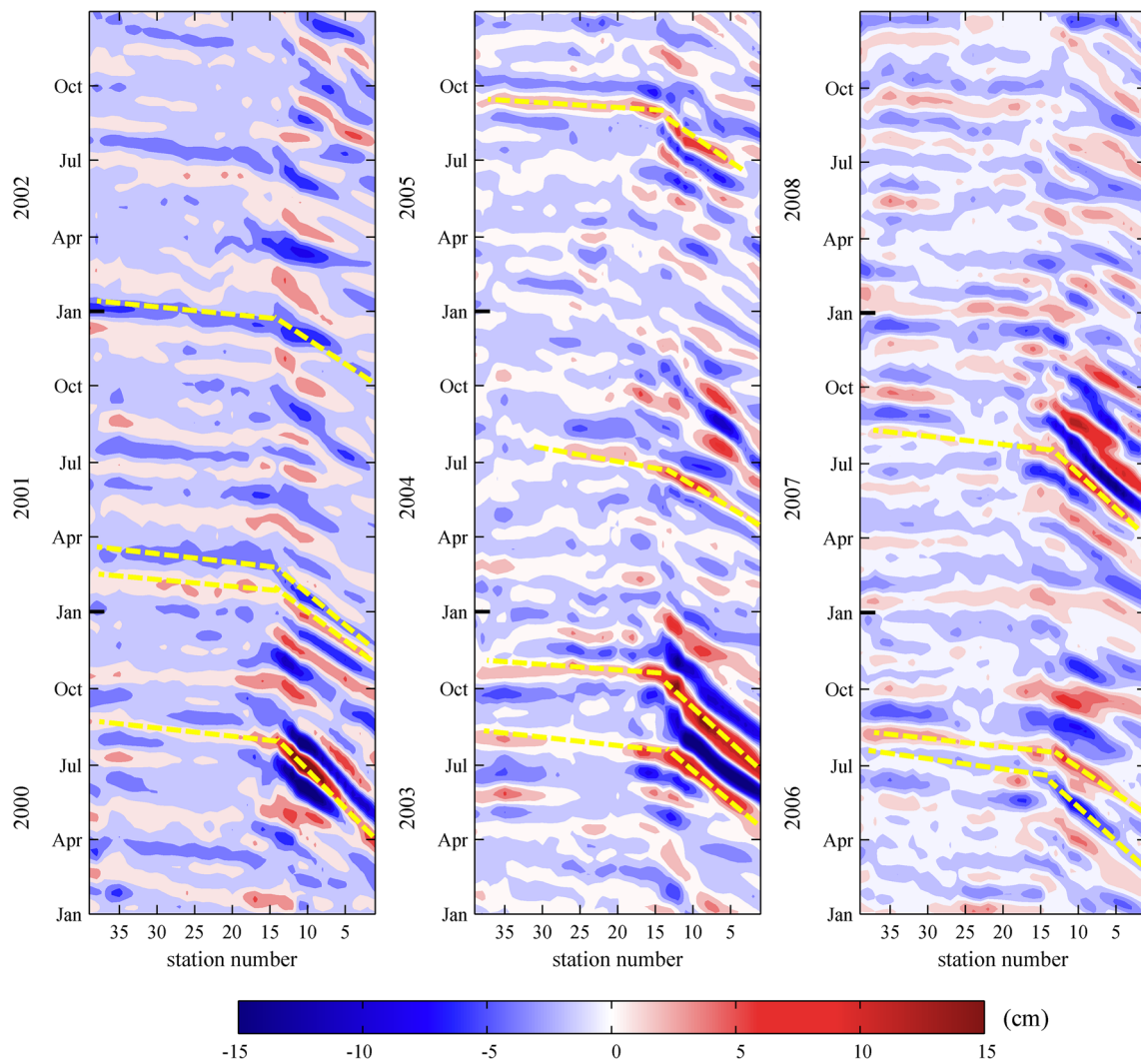


Fig. 6 Time-station diagram of intra-seasonal SLAs from the QSCAT run along the CTW waveguide shown in Fig. 5a from 2000 to 2008

Ocean (e.g., resonant oscillations in semi-enclosed seas, wobbling of the Mindanao Eddy, and MJO-related wind forcing; for more details, see Qiu et al. 1999).

The time-station diagram also indicates that not all the energy of the Rossby waves transforms into CTWs. When SLA signals reach the coast (e.g., station 14), their amplitudes decrease dramatically, from about 15 to 5 cm. Another interesting phenomenon is that the Pacific-origin SLA signals are stronger during April–October, and it will be interesting to clarify the relevant mechanisms in future studies.

4 Discussion and conclusions

For the propagating SLA signals along the Philippine Archipelago, an important factor that must be considered is

along-shore wind forcing. In order to quantify the relative importance of locally wind-forced SLA variations, we consider below the dynamic balance proposed by Enfield and Allen (1980) and Chelton and Davis (1982):

$$\frac{\partial h'}{\partial s} = \frac{\tau'_s}{\rho_0 g H_1} \tag{1}$$

where s denotes the along-shore distance, τ'_s is the along-shore component of the wind stress anomaly, ρ_0 , g and H_1 ($=50$ m) are the reference seawater density, acceleration due to gravity and depth of the thermocline, respectively. Dynamically, Eq. (1) represents the balance between the wind-induced onshore Ekman transport (if $\tau'_s > 0$) and the offshore geostrophic transport associated with the along-shore SLA gradient. Figure 7 compares the OFES SLA difference time series at each station (bottom panels) with

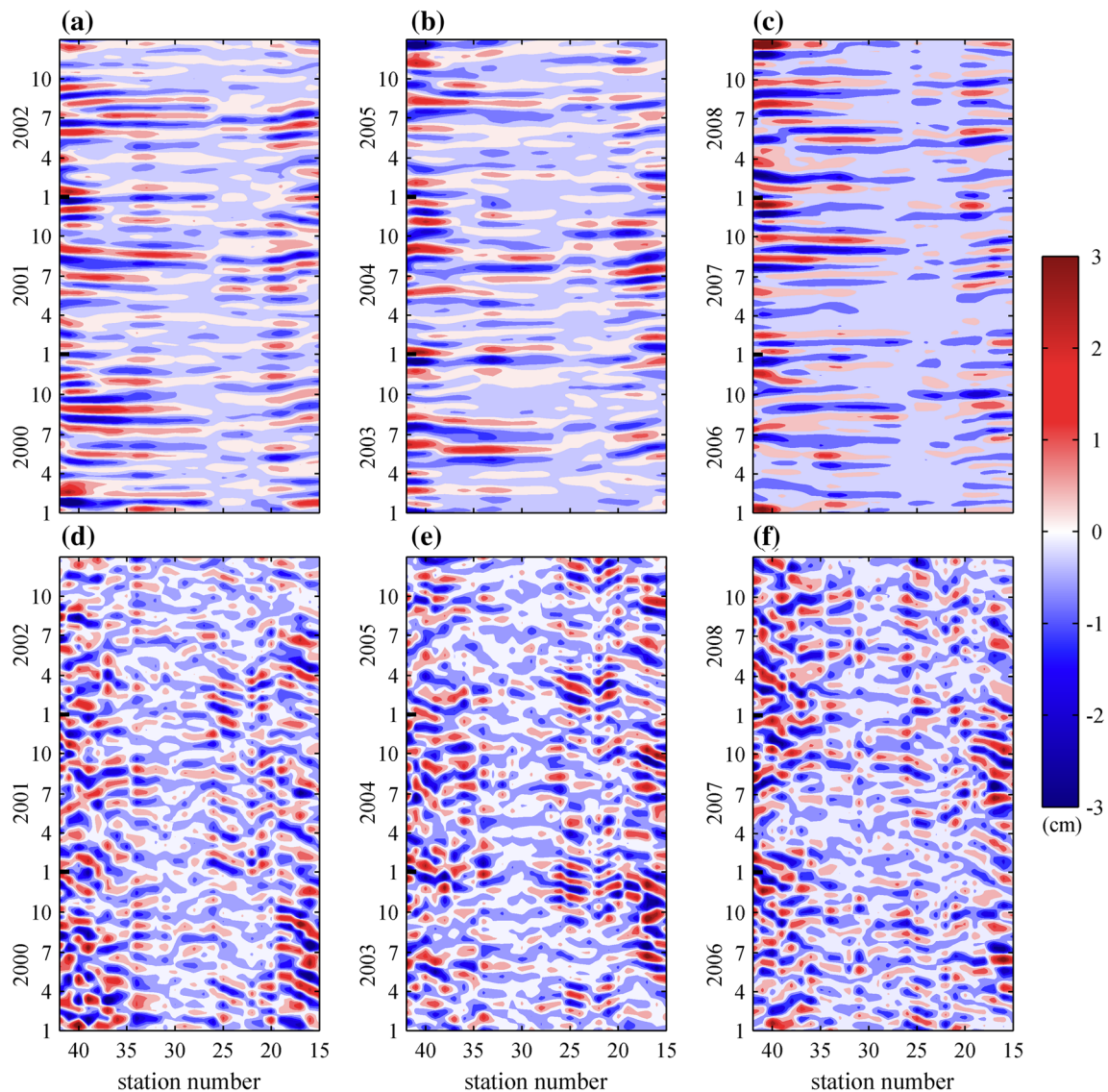


Fig. 7 Time–station diagram of the intra-seasonal SLA (cm) difference signals calculated from along-shore wind (a–c) and from the QSCAT run (d–f) at stations 15–42 from 2000 to 2008

the $\tau_s' ds / \rho_0 g H_1$ time series (top panels), where ds denotes the distance between the neighboring stations. The along-shore, wind-induced, intra-seasonal SLA signals tend to have coherent along-shore variability and their time-varying signals appear to not be in phase with those from the QSCAT run output. Figure 8 shows the linear correlation coefficient as a function of along-shore stations between the wind-induced and modeled SLA difference time series presented in Fig. 7. While the correlation coefficient can reach 0.5 at specific stations (e.g., stations 27–29 along the southern Sulu Sea), its averaged value along the CTW waveguide is ~ 0.2 . This result indicates that the interior Pacific wind forcing likely plays a more important role than the along-shore wind forcing for the

intra-seasonal SLA signals along the coast of the Philippine Archipelago.

In the above analyses, we chose one typical waveguide initiated along 12°N (Fig. 5a) to describe propagation and transformation of the intra-seasonal SLA signals. Besides this waveguide, another zonal band with large intra-seasonal SLA signals is located in the interior North Pacific Ocean along $18^\circ\text{--}28^\circ\text{N}$. Dynamically, the high eddy variability along this band is due to the unstable Subtropical Countercurrent (STCC) (Qiu 1999; Liu and Li 2007). The SLA signals generated along the STCC, however, cannot propagate southward along the west coast of the Luzon Island as CTWs and affect the intra-seasonal SLA signals in the eastern SCS. To demonstrate this point, we follow

Fig. 8 Linear correlation as a function of along-shore stations between the wind-forced intra-seasonal SLA differences signals $dh' = \tau'_s ds / \rho_0 g H_1$ and the modeled SLA difference between two neighboring stations from the QSCAT run

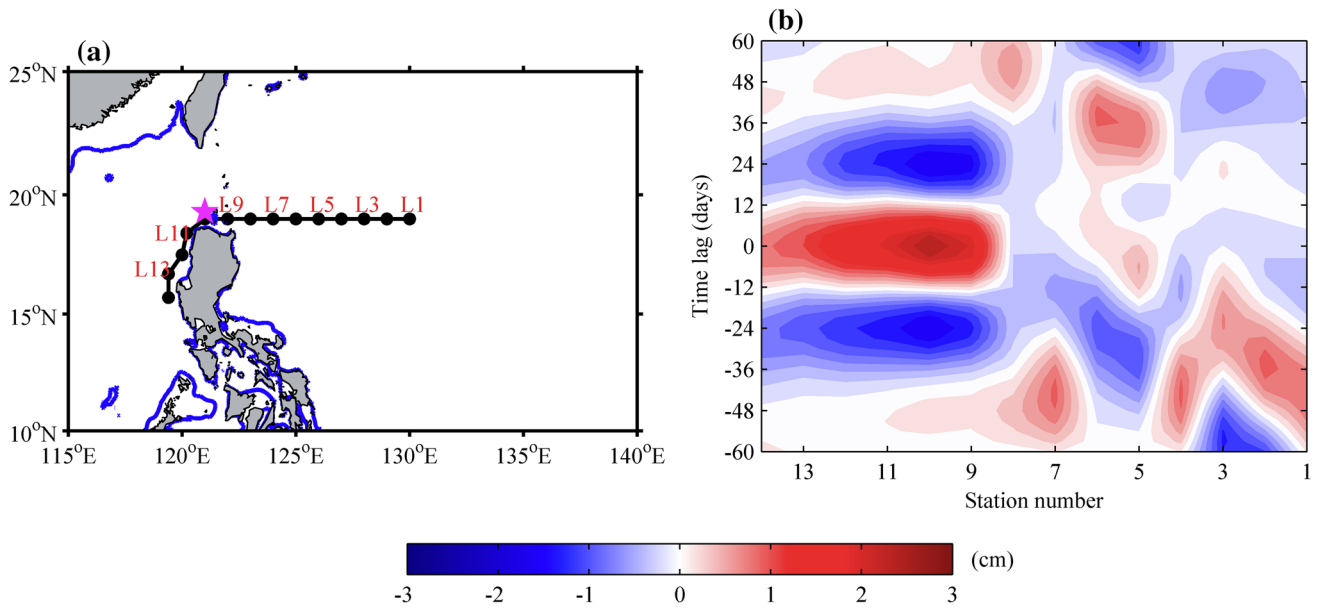
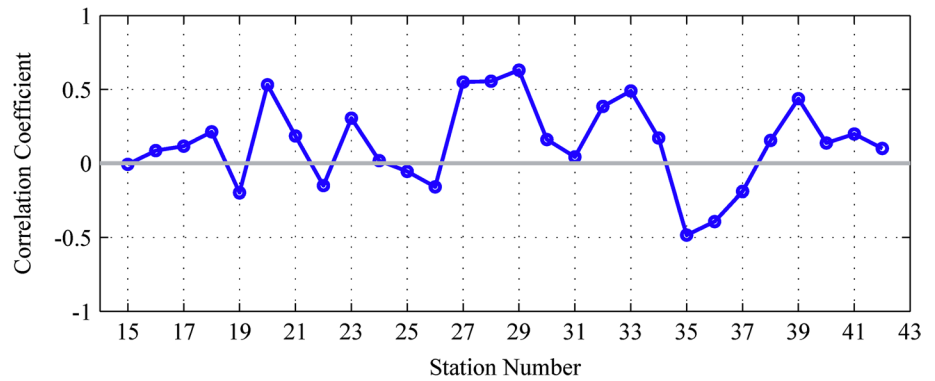


Fig. 9 **a** Distribution of 1° boxes along the Luzon path; the location of reference station L10 is indicated by a magenta star, with 100-m contours. **b** Corresponding time–station diagram of lead–lag regression

of the intra-seasonal SLA (cm) with reference to the normalized values at station L10. The 95 % confidence level has a SLA value of 0.1 cm

the methodology used in Sect. 3.2 and set up another pathway around the Luzon Strait (Fig. 9a). Using station 10 at the northern tip of the Luzon Strait as a reference site, we plot in Fig. 9b the lead–lag regressed SLA signals along the selected pathway. Unlike the southern waveguide (cf. Fig. 5d), the SLA signals along the west coast of the Luzon Island (station 10–14) do not show similar patterns of propagation. Also important from Fig. 9b is the fact that the intra-seasonal SLAs at the Luzon Strait appear to be disconnected from the SLAs originating in the interior North Pacific Ocean (i.e., stations 1–6). Across the Luzon Strait, it has been argued by many previous studies that mesoscale SLA signals deform and are absorbed by the Kuroshio (e.g., Li et al. 2007; Zhang et al. 2010; Lu and Liu 2013).

Using altimetry measurements and eddy-resolving model outputs, we investigated the connection between intra-seasonal SLAs around the Philippine Archipelago.

On an intra-seasonal time scale, the Pacific-origin SLA signals propagate westward in the form of baroclinic Rossby waves. After impinging on the east coast of the Philippines, the Rossby waves transform into CTWs, propagate clockwise along the coast and enter the eastern SCS through the Sibutu Passage and the Mindoro Strait. In addition, the Pacific-origin intra-seasonal SLA signals are stronger during April–October and the strength changes from year to year. These results suggest that intra-seasonal variability modulates both the seasonal and interannual time scales. Future studies are called for to further clarify their underlying dynamics.

Acknowledgments We acknowledge AVISO for providing SLA data (<http://www.aviso.oceanobs.com/en>). QuikSCAT data were produced by remote sensing systems and sponsored by the National Aeronautics and Space Administration (NASA) Ocean Vector Winds Science Team. Data are available at www.remss.com. The OFES

simulation was conducted on an earth simulator under the support of the Japan Agency for Marine-Earth Science and Technology (JAMSTEC). The QuikSCAT and OFES data used in this study were obtained from the Asia-Pacific Data-Research Center (APDRC), University of Hawaii (<http://apdrc.soest.hawaii.edu>). This study was supported by the Strategic Priority Research Program of the Chinese Academy of Sciences (Grant Number XDA11010103 and XDA11010203) and National Natural Science Foundation of China (Grant Number 41176024 and 41176023).

References

- Amedo CLA, Villanoy, Udarbe-Walker MJ (2002) Indicators of upwelling at the Northern Bicol Shelf, UPV. *J Nat Sci* 7:42–52
- Boyer TP, Levitus S (1997) Objective analyses of temperature and salinity for the world ocean on a 1/4° grid, NOAA Atlas NESDIS, 11. US Government Printing Office, Washington, DC
- Chelton DB, Davis RE (1982) Monthly mean sea-level variability along the west coast of North America. *J Phys Oceanogr* 12:757–784
- Chelton DB, Schlax MG (1996) Global observations of oceanic Rossby waves. *Science* 272(5259):234–238
- Chelton DB, DeSzoek RA, Schlax MG, El Naggar K, Siwertz N (1998) Geographical variability of the first baroclinic Rossby radius of deformation. *J Phys Oceanogr* 28:433–460
- Cheng X, Qi Y (2007) Trends of sea level variations in the South China Sea from merged altimetry data. *Glob Planet Chang* 57:371–382. doi:10.1016/j.gloplacha.2007.01.005
- Cheng X, Xie S-P, McCreary JP, Qi Y, Du Y (2013) Intraseasonal variability of sea surface height in the Bay of Bengal. *J Geophys Res Oceans* 118:816–830. doi:10.1002/jgrc.20075
- Dibarboure G, Lauret O, Mertz F, Rosmorduc V, Maheu C (2008) SSALTO/DUACS user handbook: (M) SLA and (M) ADT near-real time and delayed time products, Rep. CLS-DOS-NT-06.034, Aviso Altimetry, Ramonville St. Agne, France, p 39
- Du Y, Qu T (2010) Three inflow pathways of the Indonesian throughflow as seen from the simple ocean data assimilation. *Dyn Atmos Oceans*. doi:10.1016/j.dynatmoce.2010.04.001
- Durland TS, Qiu B (2003) Transmission of subinertial Kelvin waves through a strait. *J Phys Oceanogr* 33:1337–1350
- Enfield DB, Allen JS (1980) On the structure and dynamics of monthly mean sea level anomalies along the Pacific coast of North and South America. *J Phys Oceanogr* 10:557–578
- Fang G, Chen H, Wei Z, Wang Y, Wang X, Li C (2006) Trends and interannual variability of the South China Sea surface winds, surface height, and surface temperature in the recent decade. *J Geophys Res* 111:C11S16. doi:10.1029/2005JC003276
- Han W, Moore AM, Di Lorenzo E, Gordon AL, Lin J (2008) Seasonal surface ocean circulation and dynamics in the Philippine archipelago region during 2004–2008. *Dyn Atmos Oceans* 47:114–137
- Hsin Y-C, Wu C-R, Chao S-Y (2012) An updated examination of the Luzon Strait transport. *J Geophys Res* 117:C03022. doi:10.1029/2011JC007714
- Hu J, Kawanura H, Hong H, Kobashi F, Wang D (2001) 3–6 months variations of sea surface height in the South China Sea and its adjacent ocean. *J Oceanogr* 57:69–78. doi:10.1023/A:1011126804461
- Hu J, Zheng Q, Sun Z, Tai CK (2012) Penetration of nonlinear Rossby eddies into South China Sea evidenced by cruise data. *J Geophys Res* 117:C03010. doi:10.1029/2011JC007525
- Kalnay E et al (1996) The NCEP/NCAR 40-year reanalysis project. *Bull Am Meteorol Soc* 77:437–471. doi:10.1175/1520-0477077<0437:TNYRP>2.0.CO;2
- Kim YY, Qu T, Jensen T, Miyama T, Mitsudera H, Kang H-W, Ishida A (2004) Seasonal and interannual variations of the North Equatorial Current bifurcation in a high-resolution OGCM. *J Geophys Res* 109:C03040. doi:10.1029/2003JC002013
- Le Traon PY, Dibarboure G (1999) Mesoscale mapping capabilities of multi-satellite altimeter missions. *J Atmos Oceanic Technol* 16:1208–1223. doi:10.1175/1520-0426(1999)016<1208:MMCO MS>2.0.CO;2
- Li L, Jing C, Zhu DY (2007) Coupling and propagating of mesoscale sea level variability between the western Pacific and the South China Sea. *Chin Sci Bull* 52(12):1699–1707. doi:10.1007/s11434-007-0203-3
- Liang W-D, Yang YJ, Tang TY, Chuang W-S (2008) Kuroshio in the Luzon Strait. *J Geophys Res* 113:C08048. doi:10.1029/2007JC004609
- Liu Q, Li L (2007) Baroclinic stability of oceanic Rossby wave in the North Pacific subtropical eastwards contourcurrent. *Chin J Geophys* 50(1):84–93. doi:10.1002/cjg2.1013
- Liu Q, Feng M, Wang D (2011) ENSO-induced interannual variability in the southeastern South China Sea. *J Oceanogr* 67:127–133. doi:10.1007/s10872-011-0002-y
- Lu J, Liu Q (2013) Gap-leaping Kuroshio and blocking westward-propagating Rossby waves and eddy in the Luzon Strait. *J Geophys Res Oceans* 118:1170–1181. doi:10.1002/jgrc.20116
- Masumoto Y et al (2004) A fifty-year eddy-resolving simulation of the world ocean—preliminary outcomes of OFES (OGCM for the Earth simulator). *J Earth Simulator* 1:31–52
- Metzger EJ, Hurlburt H (1996) Coupled dynamics of the South China Sea, the Sulu Sea, and the Pacific Ocean. *J Geophys Res* 101:12331–12352
- Nitani H (1972) Beginning of the Kuroshio. In: Stommel H, Yashida K (eds) *Kuroshio: physical aspects of the Japan current*. Univ. of Wash. Press, Seattle, pp 129–163
- Pacanowski RC, Griffies SM (2000) MOM 3.0 manual, technical report. Geophys Fluid Dyn Lab, Princeton, NJ, p 680
- Qiu B (1999) Seasonal eddy field modulation of the North Pacific subtropical countercurrent: TOPEX/POSEIDON observations and theory. *J Phys Oceanogr* 29:2471–2486. doi:10.1175/1520-0485
- Qiu B, Chen S (2010) Interannual-to-decadal variability in the bifurcation of the North Equatorial Current off the Philippines. *J Phys Oceanogr* 40(11):2525–2538. doi:10.1175/2010JPO4462.1
- Qiu B, Chen S (2012) Multidecadal sea level and gyre circulation variability in the northwestern tropical Pacific Ocean. *J Phys Oceanogr* 42(1):193–206. doi:10.1175/JPO-D-11-061.1
- Qiu B, Lukas R (1996) Seasonal and interannual variability of the North Equatorial Current, the Mindanao Current, and the Kuroshio along the Pacific western boundary. *J Geophys Res* 101(C5):12315–12330. doi:10.1029/95JC03204
- Qiu B, Mao M, Kashino Y (1999) Intra-seasonal variability in the Indo-Pacific Throughflow and the regions surrounding the Indonesian Seas. *J Phys Oceanogr* 29:1599–1618
- Qu T, Kim YY, Yaremchuk M, Tozuka T, Ishida A, Yamagata T (2004) Can the Luzon Strait transport play a role in conveying the impact of ENSO to the South China Sea? *J Clim* 17:3644–3657. doi:10.1175/1520-0442(2004)017<3644:CLSTPA>2.0.CO;2
- Sasaki H, Nonaka M (2006) Far-reaching Hawaiian Lee countercurrent driven by wind-stress curl induced by warm SST band along the current. *Geophys Res Lett* 33:L13602. doi:10.1029/2006GL026540
- Sasaki H, Sasai Y, Kawahara S, Furuichi M, Araki F, Ishida A, Yamanaka Y, Masumoto Y, Sakuma H (2004) A series of eddy-resolving ocean simulations in the world ocean—OFES (OGCM for the Earth Simulator) project, paper presented at OCEANS 2004 Mar, Technol. Soc., Inst. of Electr. and Electr. Eng., Kobe, Japan
- Shaw P-T (1991) The seasonal variation of the intrusion of the Philippines sea water into the South China Sea. *J Geophys Res* 96(C1):821–827

- Sheremet VA (2001) Hysteresis of a western boundary current leaping across a gap*. *J Phys Oceanogr* 31(5):1247–1259
- Sprintall J, Gordon AL, Flament P, Villanoy CL (2012) Observations of exchange between the South China Sea and the Sulu Sea. *J Geophys Res* 117:C05036. doi:[10.1029/2011JC007610](https://doi.org/10.1029/2011JC007610)
- Toole JM, Millard RC, Wang Z, Pu S (1990) Observations of the Pacific north equatorial current bifurcation at the Philippine coast. *J Phys Oceanogr* 20(2):307–318. doi:[10.1175/1520-0485\(1990\)020<0307:OOTPNE>2.0.CO;2](https://doi.org/10.1175/1520-0485(1990)020<0307:OOTPNE>2.0.CO;2)
- Volkov DL, Larnicol G, Dorandeu J (2007) Improving the quality of satellite altimetry data over continental shelves. *J Geophys Res* 112:C06020. doi:[10.1029/2006JC003765](https://doi.org/10.1029/2006JC003765)
- Wang B, Wu R, Fu X (2000) Pacific-East Asia teleconnection: how does ENSO affect East Asian climate? *J Clim* 13:1517–1536
- Wang D, Liu Q, Huang RX, Du Y, Qu T (2006) Interannual variability of the South China Sea throughflow inferred from wind data and an ocean data assimilation product. *Geophys Res Lett* 33:L14605. doi:[10.1029/2006GL026316](https://doi.org/10.1029/2006GL026316)
- Wentz FJ, Smith DK, Mears CA, Gentemann CL (2001) Advanced algorithms for QuikScat and SeaWinds/AMSR. In: *Proc. Int. Geoscience and Remote Sensing Symp.*, vol 3, Sydney, Australia, IEEE, p 1097–1081
- Wyrski K (1961) Physical oceanography of the southeast Asian waters: scientific results of marine investigations of the South China Sea and the Gulf of Thailand 1959–1961, NAGA Rep. 2, Scripps Inst. of Oceanogr, La Jolla, Calif, p 195
- Xie S-P, Hu KM, Hafner J, Tokinaga H, Du Y, Huang G, Sampe T (2009) Indian Ocean capacitor effect on Indo-western Pacific climate during the summer following El Niño. *J Clim* 22(3):730–747. doi:[10.1175/2008JCLI2544.1](https://doi.org/10.1175/2008JCLI2544.1)
- Zhang Z, Zhao W, Liu Q (2010) Sub-seasonal variability of Luzon Strait Transport in a high resolution global model. *Acta Oceanol Sin* 29(3):9–17. doi:[10.1007/s13131-010-0032-0](https://doi.org/10.1007/s13131-010-0032-0)
- Zhuang W, Xie S-P, Wang D, Taguchi B, Aiki H, Sasaki H (2010) Intraseasonal variability in sea surface height over the South China Sea. *J Geophys Res* 115:C04010. doi:[10.1029/2009JC005647](https://doi.org/10.1029/2009JC005647)
- Zhuang W, Qiu B, Du Y (2013) Low-frequency western Pacific Ocean sea level and circulation changes due to the connectivity of the Philippine archipelago. *J Geophys Res Oceans*. doi:[10.1002/2013JC009376](https://doi.org/10.1002/2013JC009376)